

Quantum theory of exciton-photon coupling in photonic crystal slabs with embedded quantum wells

Dario Gerace*

*Dipartimento di Fisica “Alessandro Volta,” Università di Pavia, Via Bassi 6, I-27100 Pavia, Italy
and Institute of Quantum Electronics, ETH Zurich, 8093 Zurich, Switzerland*

Lucio Claudio Andreani

Dipartimento di Fisica “Alessandro Volta,” Università di Pavia, Via Bassi 6, I-27100 Pavia, Italy

(Dated: October 25, 2018)

A theoretical description of radiation-matter coupling for semiconductor-based photonic crystal slabs is presented, in which quantum wells are embedded within the waveguide core layer. A full quantum theory is developed, by quantizing both the electromagnetic field with a spatial modulation of the refractive index and the exciton center of mass field in a periodic piecewise constant potential. The second-quantized hamiltonian of the interacting system is diagonalized with a generalized Hopfield method, thus yielding the complex dispersion of mixed exciton-photon modes including losses. The occurrence of both weak and strong coupling regimes is studied, and it is concluded that the new eigenstates of the system are described by quasi-particles called *photonic crystal polaritons*, which can occur in two situations: (i) below the light line, when a resonance between exciton and non-radiative photon levels occurs (*guided polaritons*), (ii) above the light line, provided the exciton-photon coupling is larger than the intrinsic radiative damping of the resonant photonic mode (*radiative polaritons*). For a square lattice of air holes, it is found that the energy minimum of the lower polariton branch can occur around normal incidence. The latter result has potential implications for the realization of polariton parametric interactions in photonic crystal slabs.

PACS numbers: 71.36.+c, 42.50.Ct, 42.70.Qs, 71.35.-y

I. INTRODUCTION

The capability of engineering electron and photon states through spatial confinement leads to a control of radiation-matter interaction and to a number of interesting results in the field of solid-state cavity quantum electrodynamics (QED).¹ For example, the use of quantum-well (QW) excitons embedded in high-finesse semiconductor microcavities (MC) of the Fabry-Pérot type has allowed to observe a modification of spontaneous emission (weak coupling regime)² as well as the occurrence of a vacuum Rabi splitting (strong coupling regime).^{3,4} The latter effect arises when the radiation-matter coupling energy overcomes the damping rates of QW excitons and MC photons. Under such conditions, the elementary excitations of the system should not be described as barely excitonic or photonic, but rather as mixed radiation-matter states, called *MC polaritons*.^{5,6,7,8,9} The physics of exciton-polaritons in bulk materials had been introduced in the fifties^{10,11} and is now a textbook topic.^{12,13} The confinement of both excitons and photons with MC-embedded QWs leads to polariton states that are more easily observed, even at room temperature, and in fact MC polaritons have been a major research topic in the nineties. In 2000, the demonstration of coherent parametric processes due to polariton-polariton scattering^{14,15} opened a new area of research in the physics of MC polaritons and nonlinear optics. More recently, the experimental demonstration of Bose-Einstein condensation of MC polaritons with II-VI materials¹⁶ brings a new exciting development and demonstrates the

potentialities of radiation-matter interaction in the presence of electron and photon confinement.

Until now, little has been done to study radiation-matter interaction when high-quality QWs are combined with new routes for the tailoring of electromagnetic field in photonic crystals (PhC). These structures, which are characterized by a periodic modulation of the dielectric constant along one, two or three dimensions (1D, 2D, 3D),¹⁷ allow for an unprecedented control over the propagation and confinement of light at optical wavelengths. In particular, two-dimensional PhC embedded in a planar dielectric waveguide, commonly known as *photonic crystal slabs*, are receiving much attention because they allow for a 3D control of light and are easily realized at sub-micron length scales.^{18,19,20,21} In these systems, light propagation or confinement is controlled by the PhC structure in the 2D plane and by the dielectric discontinuity provided by the slab waveguide in the vertical direction. When QWs are embedded in a PhC slab, additional flexibility and new effects related to exciton-photon coupling are to be expected.

In this work we analyze radiation-matter interaction in PhC slabs, by considering the effects of coupling between QW excitons and photonic modes. A main goal is to study the conditions leading to the strong coupling regime and to point out the possibilities offered by PhC for *strong coupling engineering*. In the past, both experimental²² and theoretical²³ investigations of strong coupling regime in organic-based 1D PhC slabs have been reported, the theory being based on a semiclassical treatment. The same groups also reported a

joint work on 2D PhC slabs with organic active medium, in which the theoretical treatment was again based on a semiclassical solution of Maxwell's equations within a scattering matrix formalism.²⁴ Exciton-polaritons in 1D PhCs (ideal Bragg mirrors) in which one of the constituent media has a strong excitonic character were theoretically studied by using a fully classical approach.²⁵ Other theoretical works focused on polaritonic gaps in so-called phonon-polaritonic PhCs,²⁶ or on the properties of 3D arrays of quasi-zero-dimensional excitons (e.g., quantum dots) coupled to Bloch modes of the same periodic array of dielectric objects.²⁷ More recently, a purely 2D square lattice array of rods in a dielectric host medium has been theoretically studied, in which one of the two constituent media has a frequency-dependent permittivity with a pole at a resonant frequency.²⁸ Combining the effects of exciton confinement in QW structures with the 2D periodicity of the surrounding dielectric environment has been only studied in relation to the influence of Coulomb interaction on the longitudinal part of the electromagnetic field for deeply patterned PhCs with an unpatterned QW underneath the PhC region.²⁹ No experimental or theoretical work has been reported so far, to the best of our knowledge, on excitons or exciton-polaritons in semiconductor-based PhC structures that are the subject of this work.

In the present paper, the theoretical problem of exciton-photon coupling in PhC slabs is tackled by using a fully quantum-mechanical formalism for both photons and exciton states, which is described in detail. With respect to previous works on the quantum theory of exciton-polaritons in semiconductor nanostructures,^{30,31,32,33,34,35} the non-trivial spatial dependence of the dielectric constant is taken into account by quantization of the electromagnetic field in a non-homogeneous medium.^{36,37,38,39} The total hamiltonian for the coupled exciton-photon states is derived and diagonalized numerically to obtain the eigenenergies of the mixed modes. It is shown that polaritonic effects are typically stronger in PhC slabs than in MCs, due to the better field confinement provided by total internal reflection in the slab. As a consequence, larger vacuum Rabi splitting is found at exciton-photon resonance in strong coupling regime, which occurs when the exciton-photon coupling energy is larger than the intrinsic radiative linewidth of the photonic mode and the QW exciton. In this scenario, new quasi-particles form in the PhC slab, which we call *photonic crystal polaritons*. Preliminary results of the formalism presented here have been published as conference proceedings,^{40,41,42} and limited to 1D or triangular PhC lattices. In addition to the full theoretical formulation, we present here new results for a PhC slab made of a square lattice of air holes in a high-index suspended membrane. For a specific PhC slab design, a polariton angular dispersion is found which has a minimum close to normal incidence with respect to the slab surface. Such result paves the way for new exciting developments in the investigation of hybrid semiconductor

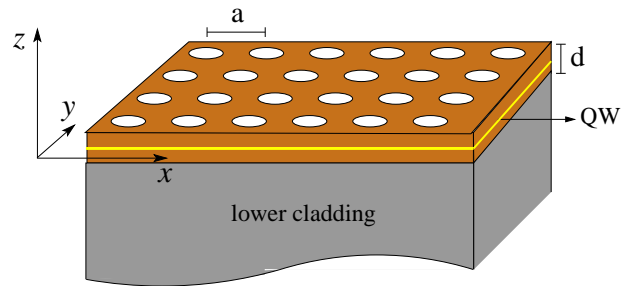


Figure 1: (color online) Schematic view of a two-dimensional photonic crystal slab of thickness d and lattice constant a , with a single quantum well grown within the core layer.

structures exhibiting both photonic and electronic band gap characteristics, as it will be discussed.

The paper is organized as follows. In Sec. II we schematically describe the system under investigation. In Sec. III we give a detailed account of the second-quantization procedure leading to the complete exciton-photon hamiltonian in the linear (low excitation density) regime and of the diagonalization technique. In Sec. IV we provide systematic results in both weak and strong coupling regimes, and describe the formation of guided and radiative polaritons. The relevance of the results in the context of parametric processes involving polariton-polariton scattering is also discussed. Finally, in Sec. V we summarize the conclusions of the work.

II. THE SYSTEM

The schematic of the model system under investigation and the choice of the coordinate axes are given in Fig. 1. We consider a high-index planar dielectric waveguide with semi-infinite cladding layers (typically the upper cladding is air). We assume that a QW of thickness L_{QW} is grown in the core of the waveguide at a certain vertical position z_{QW} , measured from the core/lower cladding interface. The dielectric material constituting the core of the planar waveguide acts also as a barrier material for the carriers (electrons and holes) confined in the thin QW layer. Typical QW thickness is of the order of $L_{\text{QW}} \simeq 10$ nm, while the dielectric core layer is usually between $d = 100$ and 200 nm thick. The QW exciton is characterized by its transition energy, E_{ex} , and by the oscillator strength per unit area, f/S .⁴³ The effect of multiple quantum wells (MQWs) grown in the core layer can be taken into account by a total oscillator strength given by the sum of single QW oscillator strengths. This approach is valid as long as $L_{\text{QW}} \ll d$, and the electric field of the relevant photonic mode can be considered as uniform along the MQW thickness. We disregard the difference in dielectric constants between QW and barrier media, and assume the core layer to be described by a relative dielectric permeability ϵ_{diel} . The core layer is patterned with a given photonic lattice, e.g. with lattice

constant a , down to the interface with the lower cladding medium. Thus, exciton center-of-mass eigenfunctions are not free as in usual QWs, but are subject to a further confining potential provided by the etched air regions. As a general remark, it is clear that exciton and photon wavefunctions are confined in the vertical direction and are subject to effective potentials having the same spatial periodicity in the 2D plane. Roughly speaking, we could say that confined excitons and photons display the same dimensionality in this problem, thereby satisfying the condition for possible occurrence of quasi-stationary, strongly coupled polariton states.^{9,44}

III. QUANTUM THEORY OF EXCITON-PHOTON COUPLING

In this Section, we detail the full quantum theory of radiation-matter interaction for QWs embedded in a PhC slab. We start by the second quantization of the electromagnetic field in a non-uniform dielectric environment, to which end we follow the treatment given in Ref. 37. Then, we quantize the exciton field by solving the Schrödinger equation for the center-of-mass QW exciton wavefunction in a periodic, piecewise constant potential. The solutions for the non-interacting fields are used to derive the coupling hamiltonian. The total hamiltonian is then diagonalized, leading to PhC polariton eigenmodes.

A. Quantized photon field in non-uniform dielectric medium: normal mode expansion

The canonical quantization of the electromagnetic field in a non-uniform dielectric medium with relative perme-

ability $\epsilon(\mathbf{r})$ (we assume a unit magnetic permeability) is carried out through quantization of the vector potential \mathbf{A} , defined from the usual relations to the fields

$$\mathbf{E}(\mathbf{r}, t) = -\frac{1}{c} \frac{\partial \mathbf{A}(\mathbf{r}, t)}{\partial t} = -\frac{1}{c} \dot{\mathbf{A}}(\mathbf{r}, t), \quad (1)$$

$$\mathbf{B}(\mathbf{r}, t) = \nabla \times \mathbf{A}(\mathbf{r}, t), \quad (2)$$

and which must satisfy the equation of motion

$$\nabla \times \nabla \times \mathbf{A} = \frac{\omega^2}{c^2} \epsilon(\mathbf{r}) \mathbf{A}. \quad (3)$$

We are considering only the retarded electromagnetic field (no scalar potential, $\Phi = 0$) and the vector potential can be chosen to satisfy the generalized Coulomb gauge³⁷

$$\nabla \cdot (\epsilon(\mathbf{r}) \mathbf{A}(\mathbf{r}, t)) = 0. \quad (4)$$

The second-quantized hamiltonian of the free photon field is straightforwardly obtained from the classical expression of the total electromagnetic energy

$$\mathcal{H}_{\text{e.m.}} = \frac{1}{8\pi} \int_V [\epsilon(\mathbf{r}) \mathbf{E}(\mathbf{r})^2 + \mathbf{B}(\mathbf{r})^2] d\mathbf{r}, \quad (5)$$

which can be derived from the Proca Lagrangian density⁴⁵ and can be expressed in terms of $\mathbf{A}(\mathbf{r}, t)$ and its conjugate momentum $\Pi(\mathbf{r}, t) = \epsilon(\mathbf{r}) \dot{\mathbf{A}}(\mathbf{r}, t)/c^2$. The field operator is expanded in normal modes as

$$\hat{\mathbf{A}}(\mathbf{r}, t) = \sum_{\mathbf{k}, n} (2\pi \hbar \omega_{\mathbf{k}n})^{1/2} \left[\hat{a}_{\mathbf{k}n} \mathbf{A}_{\mathbf{k}n}(\mathbf{r}) e^{-i\omega_{\mathbf{k}n}t} + \hat{a}_{\mathbf{k}n}^\dagger \mathbf{A}_{\mathbf{k}n}^*(\mathbf{r}) e^{i\omega_{\mathbf{k}n}t} \right], \quad (6)$$

in which $\hat{a}_{\mathbf{k}n}^\dagger$ ($\hat{a}_{\mathbf{k}n}$) are creation (destruction) operators of field quanta with eigenenergies $\omega_{\mathbf{k}n}$, and the index n is a generic band number labelling the corresponding photonic eigenmode at in-plane Bloch vector \mathbf{k} . In order to satisfy Bose commutation relations for the operators,

$$[\hat{a}_{\mathbf{k}n}, \hat{a}_{\mathbf{k}'n'}^\dagger] = \delta_{\mathbf{k}, \mathbf{k}'} \delta_{n, n'}, \quad [\hat{a}_{\mathbf{k}n}, \hat{a}_{\mathbf{k}'n'}] = [\hat{a}_{\mathbf{k}n}^\dagger, \hat{a}_{\mathbf{k}'n'}^\dagger] = 0, \quad (7)$$

the correct orthonormality condition for the classical functions $\mathbf{A}_{\mathbf{k}n}(\mathbf{r})$ satisfying Eq. (3) is^{36,37,39}

$$\int_V \epsilon(\mathbf{r}) \mathbf{A}_{\mathbf{k}n}^*(\mathbf{r}) \cdot \mathbf{A}_{\mathbf{k}'n'}(\mathbf{r}) d\mathbf{r} = \frac{c^2}{\omega_{\mathbf{k}n}^2} \delta_{\mathbf{k}, \mathbf{k}'} \delta_{n, n'}, \quad (8)$$

where V is the same quantization volume as in (5). This implies the following conditions for the electric and magnetic fields:

$$\int_V \epsilon(\mathbf{r}) \mathbf{E}_{\mathbf{k}n}^*(\mathbf{r}) \cdot \mathbf{E}_{\mathbf{k}'n'}(\mathbf{r}) d\mathbf{r} = \delta_{\mathbf{k}, \mathbf{k}'} \delta_{n, n'}, \quad (9)$$

$$\int_V \mathbf{B}_{\mathbf{k}n}^*(\mathbf{r}) \cdot \mathbf{B}_{\mathbf{k}'n'}(\mathbf{r}) d\mathbf{r} = \delta_{\mathbf{k}, \mathbf{k}'} \delta_{n, n'}. \quad (10)$$

The usual Maxwell equations for \mathbf{E} and \mathbf{B} can be derived from the equations of motion for the conjugate variables $\mathbf{A}(\mathbf{r})$ and $\Pi(\mathbf{r})$. From Eq. (5) and using the field expansion (6), we finally get the second-quantized hamiltonian of the free photon field in the usual form as a sum

of harmonic degrees of freedom,

$$\hat{H}_{\text{ph}} = \sum_{\mathbf{k}, n} \hbar \omega_{\mathbf{k}n} \left(\hat{a}_{\mathbf{k}n}^\dagger \hat{a}_{\mathbf{k}n} + \frac{1}{2} \right). \quad (11)$$

In order to implement the formalism, we shall need specific forms for the classical fields functions. The exact solution of Maxwell equations in a PhC slab is a complicated task, especially concerning quasi-guided modes that lie above the light line.^{18,19} A recently developed guided-mode expansion (GME) approach⁴⁶ allows us to find a convenient solution to this problem after expansion of the classical fields on the basis of guided modes of an effective planar waveguide. We start from the second-order equation for the magnetic field $\mathbf{B} \equiv \mathbf{H}$ in a source-free dielectric medium and for harmonic time dependence,

$$\nabla \times \left[\frac{1}{\epsilon(\mathbf{r})} \nabla \times \mathbf{H} \right] = \frac{\omega^2}{c^2} \mathbf{H}. \quad (12)$$

Due to the in-plane translational invariance implying Bloch-Floquet theorem, the magnetic field can be expanded on a basis in which planar and vertical coordinates are factorized

$$\mathbf{H}_{\mathbf{k}}(\mathbf{r}) = \sum_{\mathbf{G}} \sum_{\alpha} c_{\mathbf{k}, \alpha}(\mathbf{G}) \mathbf{h}_{\mathbf{k}+\mathbf{G}, \alpha}(z) e^{i(\mathbf{k}+\mathbf{G}) \cdot \boldsymbol{\rho}}, \quad (13)$$

where $\mathbf{r} = (\boldsymbol{\rho}, z)$, \mathbf{k} is the in-plane Bloch vector in the first Brillouin zone (BZ), \mathbf{G} are reciprocal lattice vectors, and the functions $\mathbf{h}_{\mathbf{k}+\mathbf{G}, \alpha}(z)$ ($\alpha = 1, 2, \dots$) are the (discrete) guided modes of the effective planar waveguide with an average dielectric constant in each layer, calculated from the air fraction of the given photonic lattice. Thus, Eq. (12) is reduced to a linear eigenvalue problem

$$\sum_{\mathbf{G}'} \sum_{\alpha'} \mathcal{M}_{\mathbf{k}+\mathbf{G}, \mathbf{k}+\mathbf{G}'}^{\alpha, \alpha'} c_{\alpha'}(\mathbf{k} + \mathbf{G}') = \frac{\omega^2}{c^2} c_{\alpha}(\mathbf{k} + \mathbf{G}), \quad (14)$$

which is solved by diagonalizing the explicit expression for the matrix \mathcal{M} .⁴⁶ The properties of the specific photonic lattice enter in the matrix \mathcal{M} as a Fourier transform of the inverse dielectric constant in each layer, $\eta(\mathbf{G}, \mathbf{G}') = \epsilon^{-1}(\mathbf{G}, \mathbf{G}')$, the matrix inversion being performed numerically. After diagonalization, the resulting photonic modes can be classified according to their band index, n , and their in-plane Bloch vector \mathbf{k} . It should be noted that the classical fields $\mathbf{H}_{\mathbf{k}n}(\mathbf{r})$ and $\mathbf{E}_{\mathbf{k}n}(\mathbf{r}) = ic/(\omega\epsilon(\mathbf{r}))\nabla \times \mathbf{H}_{\mathbf{k}n}(\mathbf{r})$ calculated by the GME approach automatically satisfy the orthonormality conditions (9-10), thus they constitute a very convenient set for

the second-quantized formulation. Finally, we point out that losses of a quasi-guided photonic eigenmode can be introduced in the present treatment as an imaginary part $\gamma_{\mathbf{k}n}$ of mode eigenenergies. Such imaginary part arises for modes lying above the light line from out-of-plane diffraction losses, which are calculated in perturbation theory as detailed in Ref. 46.

B. Quantized exciton field in a periodic piecewise constant potential

Exciton confinement in QWs has been widely investigated in the past (for a review see, e.g., Ref. 43). Also, second-quantization of the QW exciton field has been extensively treated in the literature. Two recent approaches leading to an effective hamiltonian of interacting bosons starting from the full crystal hamiltonian are given in Refs. 47,48. When the exciton density n_{ex} is low, i.e., much smaller than a saturation density $n_{\text{sat}} \simeq 1/(2\pi a_{2D}^2)$ (where a_{2D} is the 2D exciton Bohr radius),^{49,50} QW excitons behave as a gas of non-interacting bosons to a very good approximation.

The envelope function $F(\mathbf{r}_e, \mathbf{r}_h)$ of QW excitons can be factorized in a wavefunction depending on a center-of-mass coordinate \mathbf{R}_{\parallel} and an electron-hole wavefunction depending on the in-plane relative coordinate $\boldsymbol{\rho}$ as

$$F(\mathbf{r}_e, \mathbf{r}_h) = F_{\mathbf{K}}(\mathbf{R}_{\parallel}) f(\boldsymbol{\rho}, z_e, z_h), \quad (15)$$

where $F_{\mathbf{K}}(\mathbf{R}_{\parallel}) = e^{i\mathbf{K} \cdot \mathbf{R}_{\parallel}}$ for free QW excitons. Considering the system of Fig. 1, the QW layer is patterned with a photonic lattice of air holes and the center-of-mass wavefunction $F_{\mathbf{K}}(\mathbf{R}_{\parallel})$ for exciton motion in the 2D plane is not a simple plane wave anymore.⁵¹ This wavefunction obeys a Schrödinger equation

$$\left[-\frac{\hbar^2 \nabla^2}{2M_{\text{ex}}} + V(\mathbf{R}_{\parallel}) \right] F_{\mathbf{K}}(\mathbf{R}_{\parallel}) = E_{\mathbf{K}} F_{\mathbf{K}}(\mathbf{R}_{\parallel}), \quad (16)$$

where $M_{\text{ex}} = m_e^* + m_h^*$ is the total exciton mass and the potential $V(\mathbf{R}_{\parallel}) = 0$ in the non-patterned regions, while $V(\mathbf{R}_{\parallel})$ takes a large value V_{∞} in the air holes. Equation (16) can be solved by plane-wave expansion,

$$F_{\mathbf{K}}(\mathbf{R}_{\parallel}) = \sum_{\mathbf{G}} F(\mathbf{K} + \mathbf{G}) e^{i(\mathbf{K}+\mathbf{G}) \cdot \mathbf{R}_{\parallel}}, \quad (17)$$

where the exciton wavevector \mathbf{K} is now restricted to the first Brillouin zone and \mathbf{G} are the same reciprocal vectors of the photonic lattice. The resulting equation in Fourier space is

$$\sum_{\mathbf{G}'} \left[\frac{\hbar^2 |\mathbf{k} + \mathbf{G}'|^2}{2M_{\text{ex}}} \delta_{\mathbf{G}, \mathbf{G}'} + V(\mathbf{G} - \mathbf{G}') \right] F(\mathbf{K} + \mathbf{G}') = E_{\mathbf{K}} F(\mathbf{K} + \mathbf{G}), \quad (18)$$

where the Fourier matrix $V(\mathbf{G}, \mathbf{G}') \equiv V(\mathbf{G} - \mathbf{G}')$ has expressions similar to those for $\epsilon(\mathbf{G}, \mathbf{G}')$ in the photonic problem. Equation (18) is solved numerically, yielding quantized center-of-mass levels in the periodic potential. By this procedure, the exciton levels are labelled by the same quantum numbers as the electromagnetic modes, namely a Bloch vector \mathbf{K} and a discrete index ν . The exciton energy is written as $E_{\mathbf{K}\nu}^{(\text{ex})} = E_{\text{ex}} + E_{\mathbf{K}\nu}$, where E_{ex} is the bare QW exciton energy (which is given for the specific QW parameters), while $E_{\mathbf{K}\nu}$ is the center-of-mass quantization energy in the in-plane potential $V(\mathbf{R}_{\parallel})$. It turns out that $E_{\mathbf{K}\nu} \sim 10^{-2} - 10^{-1}$ meV for typical PhC slab patterns, depending on a and r/a . Now we may introduce exciton creation (destruction) operators for center-of-mass eigenmodes, $\hat{b}_{\mathbf{K}\nu}^{\dagger}$ ($\hat{b}_{\mathbf{K}\nu}$). In second quantization, the hamiltonian of the bare exciton field is finally given by

$$\hat{H}_{\text{ex}} = \sum_{\mathbf{K}, \nu} E_{\mathbf{K}\nu}^{(\text{ex})} \hat{b}_{\mathbf{K}\nu}^{\dagger} \hat{b}_{\mathbf{K}\nu}, \quad (19)$$

where for $n_{\text{ex}} \ll 1/a_D^2$ the excitonic operators obey commutation relations

$$[\hat{b}_{\mathbf{K}\nu}, \hat{b}_{\mathbf{K}'\nu'}^{\dagger}] \simeq \delta_{\mathbf{K}, \mathbf{K}'} \delta_{\nu, \nu'}, \quad [\hat{b}_{\mathbf{K}\nu}, \hat{b}_{\mathbf{K}'\nu'}] = [\hat{b}_{\mathbf{K}\nu}^{\dagger}, \hat{b}_{\mathbf{K}'\nu'}^{\dagger}] \simeq 0. \quad (20)$$

Broadening of the exciton spectral lines can be taken into account phenomenologically by introducing an imaginary part of mode energies γ_{ex} , taken as a \mathbf{K} - and ν -independent parameter.

C. Exciton-photon interaction hamiltonian

The interaction between exciton and photon states must conserve the Bloch vector, i.e., $\mathbf{K} = \mathbf{k}$ (modulo a reciprocal lattice vector). Thus, we will use the same notation for exciton and photon wave vectors. However, in general a photonic mode with band index n couples to exciton center-of-mass levels with any ν . The interaction is determined by a matrix element of the full hamiltonian, as first shown in Refs. 10,11 for bulk exciton-polaritons and later extended to quantum-confined systems.^{30,33,34,35} The classical minimal coupling hamiltonian is given by

$$\mathcal{H}_I = -\frac{e}{2m_0c} \sum_{j=1}^N \{ \mathbf{A}(\mathbf{r}_j) \cdot \mathbf{p}_j + \mathbf{p}_j \cdot \mathbf{A}(\mathbf{r}_j) \} + \frac{e^2}{2m_0c^2} \sum_{j=1}^N |\mathbf{A}(\mathbf{r}_j)|^2, \quad (21)$$

where m_0 is the free electron mass, \mathbf{r}_j (\mathbf{p}_j) are the position (momentum) variables of the QW electrons, and the sum runs over all the electrons in the system. In Eq. (21), we have retained both $\mathbf{A} \cdot \mathbf{p}$ and $\mathbf{p} \cdot \mathbf{A}$ terms, because the generalized Coulomb gauge (4) does not allow in general for the commutation of these two operators. Taking into account the presence of a non-local potential, we can write this hamiltonian in second-quantized form as $\hat{H}_I = \hat{H}_I^{(1)} + \hat{H}_I^{(2)}$, where the two contributions are^{52,53}

$$\hat{H}_I^{(1)} = i \frac{e}{\hbar c} \sum_{j=1}^N \hat{\mathbf{A}}(\mathbf{r}_j) \cdot [\hat{\mathbf{r}}_j, \hat{H}_{\text{ex}}], \quad (22)$$

$$\hat{H}_I^{(2)} = -i \frac{e^2}{2\hbar c^2} \sum_{j=1}^N [\hat{\mathbf{A}}(\mathbf{r}_j) \cdot \hat{\mathbf{r}}_j, \hat{\mathbf{A}}(\mathbf{r}_j) \cdot \hat{\mathbf{v}}_j], \quad (23)$$

and the operator $\hat{\mathbf{v}}_j = \hat{\mathbf{p}}_j/m_0 = (i\hbar)^{-1}[\hat{\mathbf{r}}_j, \hat{H}_{\text{ex}}]$ directly follows from Heisenberg equation of motion for $\hat{\mathbf{r}}_j$. Introducing exciton operators and resolving the commutator,

one can write, e.g., for the first term

$$\hat{H}_I^{(1)} = -i \frac{e}{\hbar c} \sum_{\mathbf{k}, \nu} E_{\mathbf{k}\nu}^{(\text{ex})} \langle \Psi_{\mathbf{k}\nu}^{(\text{ex})} | \sum_j \hat{\mathbf{A}}(\mathbf{r}_j) \cdot \mathbf{r}_j | 0 \rangle \hat{b}_{\mathbf{k}\nu}^{\dagger} + \text{h.c.}, \quad (24)$$

where $\Psi_{\mathbf{k}\nu}^{(\text{ex})}$ is the many-body exciton wavefunction while $|0\rangle$ is the crystal ground state. Expanding the vector potential as in Eq. (6), and expressing also $\hat{H}_I^{(2)}$ in terms of exciton operators, after some manipulation the two terms of the second-quantized interaction hamiltonian are obtained in the form

$$\hat{H}_I^{(1)} = i \sum_{\mathbf{k}, n, \nu} C_{\mathbf{k}n\nu} (\hat{a}_{\mathbf{k}n} + \hat{a}_{-\mathbf{k}n}^{\dagger}) (\hat{b}_{-\mathbf{k}\nu} - \hat{b}_{\mathbf{k}\nu}^{\dagger}), \quad (25)$$

$$\hat{H}_I^{(2)} = \sum_{\mathbf{k}, \nu, n, n'} D_{\mathbf{k}\nu nn'} (\hat{a}_{-\mathbf{k}n} + \hat{a}_{\mathbf{k}n}^{\dagger}) (\hat{a}_{\mathbf{k}n'} + \hat{a}_{-\mathbf{k}n'}^{\dagger}) \quad (26)$$

The coupling matrix element $C_{\mathbf{k}n\nu}$ between exciton and photon states at a given \mathbf{k} is calculated as⁵⁴

$$C_{\mathbf{k}n\nu} = E_{\mathbf{k}\nu}^{(\text{ex})} \left(\frac{2\pi e^2 \hbar \omega_{\mathbf{k}n}}{\hbar^2 c^2} \right)^{1/2} \langle \Psi_{\mathbf{k}\nu}^{(\text{ex})} | \sum_j \mathbf{A}_{\mathbf{k}n}(\mathbf{r}_j) \cdot \mathbf{r}_j | 0 \rangle, \quad (27)$$

while $D_{\mathbf{k}\nu n n'} = C_{\mathbf{k}\nu}^* C_{\mathbf{k}n' \nu} / E_{\mathbf{k}\nu}^{(\text{ex})}$.

The integral in Eq. (27) can be expressed in terms of the oscillator strength f of the excitonic transition, which is generally defined as⁴³

$$f_{\hat{\mathbf{e}}} = \frac{2m_0\Omega_{\text{ex}}}{\hbar} |\langle \Psi_{\mathbf{k}\nu}^{(\text{ex})} | \hat{\mathbf{e}} \cdot \sum_j \mathbf{r}_j | 0 \rangle|^2, \quad (28)$$

where $\Omega_{\text{ex}} = E_{\mathbf{k}\nu}^{(\text{ex})} / \hbar$ and $\hat{\mathbf{e}}$ is the polarization unit vector of the exciton. For a QW exciton the oscillator strength per unit area is calculated as

$$\frac{f_{\hat{\mathbf{e}}}}{S} = \frac{2m_0\Omega_{\text{ex}}}{\hbar} |\hat{\mathbf{e}} \cdot \mathbf{r}_{\text{cv}}|^2 \left| \int f(\boldsymbol{\rho} = 0, z, z) dz \right|^2, \quad (29)$$

in which $\mathbf{r}_{\text{cv}} = \langle u_{\text{c0}} | \mathbf{r} | u_{\text{v0}} \rangle$ is the dipole matrix element between the single-particle Bloch functions in the valence and conduction bands of the bulk crystal. We are considering the ground-state heavy-hole (HH) exciton, whose optically active states are polarized in the xy plane and are doubly degenerate. Thus, HH QW excitons preferentially couple to TE-like modes in the photonic structure. Expressing the exciton wave function in terms of the QW envelope function (15), it is easy to see that the coupling energy (27) depends on the oscillator strength per unit area, Eq. (29), as well as on the spatial overlap between the exciton center-of-mass wavefunction and the photonic mode profile in the QW plane. Assuming the mode profile to be uniform along the QW thickness, we can express the coupling matrix element as⁵⁴

$$C_{\mathbf{k}\nu} \simeq -i \left(\frac{\pi \hbar^2 e^2 f}{m_0 S} \right)^{1/2} \int \hat{\mathbf{e}} \cdot \mathbf{E}_{\mathbf{k}n}(\boldsymbol{\rho}, z_{\text{QW}}) F_{\mathbf{k}\nu}^*(\boldsymbol{\rho}) d\boldsymbol{\rho}, \quad (30)$$

where we approximated $E_{\mathbf{k}\nu}^{(\text{ex})} \simeq \hbar\omega_{\mathbf{k}n}$, assuming close-to-resonance coupling.⁵⁵ We notice that for MQWs the coupling energy (30) can be multiplied by $\sqrt{N_{\text{QW}}}$, where N_{QW} is the effective number of QWs coupled to the photonic mode. Within our GME formalism, the integral in Eq. (30) can be straightforwardly calculated in Fourier space and we finally get

$$C_{\mathbf{k}\nu} \simeq -i \left(\frac{\pi \hbar^2 e^2 f}{m_0 S} \right)^{1/2} \sum_{\mathbf{G}} \hat{\mathbf{e}} \cdot \mathbf{E}_{\mathbf{k}+\mathbf{G},n}(z_{\text{QW}}) F_{\mathbf{k}+\mathbf{G},\nu}^*, \quad (31)$$

where $\mathbf{E}_{\mathbf{k}+\mathbf{G},n}(z_{\text{QW}})$ is the Fourier transform of the mode electric field at the QW vertical position.⁵⁶ Thus, all parameters of the interaction hamiltonian are obtained in terms of the electric field coefficients calculated by the GME method and of the exciton coefficients corresponding to quantized center-of-mass levels.

D. Diagonalization of the total hamiltonian

The full quantum hamiltonian describing the coupled QW exciton and PhC slab modes is given by

$$\hat{H}_{\text{tot}} = \hat{H}_{\text{ph}} + \hat{H}_{\text{ex}} + \hat{H}_{\text{I}}^{(1)} + \hat{H}_{\text{I}}^{(2)}, \quad (32)$$

where \hat{H}_{ph} , \hat{H}_{ex} and the two interaction hamiltonians are explicitly given in Eqs. (11), (19), and (25)-(26). In the bare photonic dispersion, we do not consider the zero-point energy term. Not surprisingly, Eq. (32) has a formal analogy with the second-quantized exciton-photon hamiltonian in bulk,¹⁰ planar MCs,³⁰ or pillar MCs.³⁵ Such hamiltonian is valid in the linear regime, i.e., under low excitation. Non-linear terms including exciton-exciton scattering and saturation of exciton-photon coupling^{49,50} are not considered here.

The total hamiltonian of the exciton-photon coupled system is diagonalized by using a generalized Hopfield transformation.^{10,30,34,35} New destruction (creation) operators $\hat{p}_{\mathbf{k}}$ ($\hat{p}_{\mathbf{k}}^\dagger$) are defined as

$$\hat{p}_{\mathbf{k}} = \sum_n w_{\mathbf{k}n} a_{\mathbf{k}n} + \sum_\nu x_{\mathbf{k}\nu} b_{\mathbf{k}\nu} + \sum_n y_{\mathbf{k}n} a_{-\mathbf{k}n}^\dagger + \sum_\nu z_{\mathbf{k}\nu} b_{-\mathbf{k}\nu}^\dagger, \quad (33)$$

which still satisfy Bose commutation relations

$$[\hat{p}_{\mathbf{k}}, \hat{p}_{\mathbf{k}'}^\dagger] = \delta_{\mathbf{k},\mathbf{k}'}, \quad [\hat{p}_{\mathbf{k}}, \hat{p}_{\mathbf{k}'}] = [\hat{p}_{\mathbf{k}}^\dagger, \hat{p}_{\mathbf{k}'}^\dagger] = 0. \quad (34)$$

The condition for the total hamiltonian to be diagonal in terms of $\hat{p}_{\mathbf{k}}$, $\hat{p}_{\mathbf{k}}^\dagger$ is

$$[\hat{p}_{\mathbf{k}}, \hat{H}_{\text{tot}}] = \hbar\Omega_{\mathbf{k}} \hat{p}_{\mathbf{k}}. \quad (35)$$

The transformation, which leads to a non-hermitian eigenvalue problem, applies also to a hamiltonian that includes dissipative terms. This is the present case when the imaginary part of the frequency for quasi-guided photonic modes, as well as the exciton linewidth arising from non-radiative processes, are included in the terms \hat{H}_{ph} , \hat{H}_{ex} of Eq. (32). The eigenvalue problem can be written in the form

$$\mathbb{M}_{\mathbf{k}} \vec{\mathbf{v}}_{\mathbf{k}} = \hbar\Omega_{\mathbf{k}} \vec{\mathbf{v}}_{\mathbf{k}}, \quad (36)$$

where $\mathbb{M}_{\mathbf{k}}$ is the generalized Hopfield matrix at a specific wave vector \mathbf{k} , and $\vec{\mathbf{v}}_{\mathbf{k}}$ is a generalized vector constituted by the expansion coefficients of Eq. (33) (see Appendix). Diagonalization of Eq. (36) gives directly the complex eigenenergies $\hbar\Omega_{\mathbf{k}}$ corresponding to mixed excitations of radiation and matter. Depending on the interplay between exciton-photon coupling and their respective losses, the system can be either in a weak or in a strong-coupling regime. In the latter case, $\hbar\Omega_{\mathbf{k}}$ calculated for any \mathbf{k} in the first BZ gives rise to the full spectrum of *photonic crystal polaritons*.

IV. NUMERICAL RESULTS: THE SQUARE LATTICE PHC SLAB

In this Section we apply the present theory to a square lattice of air holes in a symmetric PhC slab with air claddings. We consider a GaAs membrane with a dielectric constant $\epsilon_{\text{diel}} = 12.46$, typical of this material in the near infrared. A schematic representation of the direct

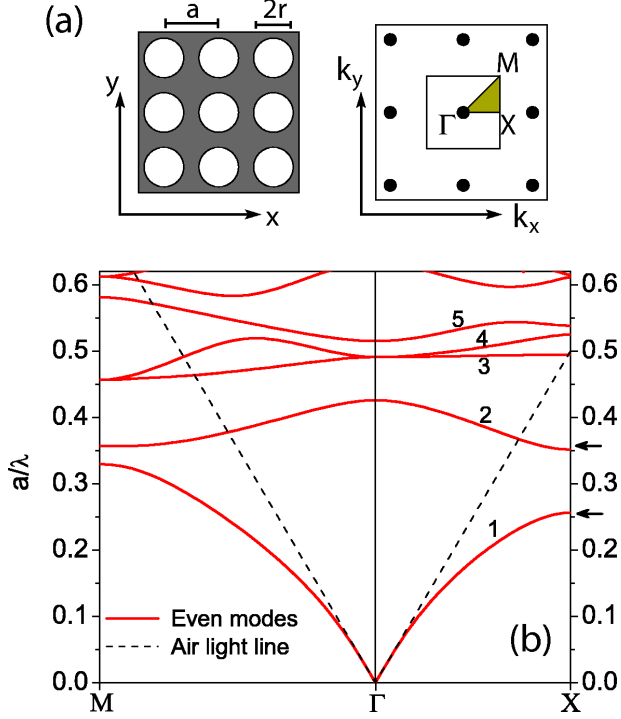


Figure 2: (color online) (a) Square lattice of air holes: direct and reciprocal lattices with Brillouin zone and main symmetry points, (b) photonic mode dispersion (even modes, $\sigma_{xy} = +1$) when the lattice is embedded in a high-index ($n_{\text{diel}} = 3.43$) photonic crystal membrane. Parameters are: $r/a = 0.34$, $d/a = 0.3$. The first few modes are labelled by a band number. Dashed lines represent the light dispersion in air.

and reciprocal lattices is shown in Fig. 2(a). The photonic lattice is characterized by the inter-hole separation, a , and the hole radius, r . In reciprocal space, the BZ is evidenced and the main symmetry points Γ , X , and M are defined. In Fig. 2(b) we show a typical photonic band diagram calculated by using the GME method,⁴⁶ for a PhC membrane with thickness $d/a = 0.3$ and hole radius $r/a = 0.34$. The dispersion is shown in dimensionless frequency units [$\omega a/(2\pi c) = a/\lambda$], and only for modes with even parity ($\sigma_{xy} = +1$) with respect to a horizontal mirror plane at the middle of the slab. Such modes have mainly in-plane polarized electric field (also defined TE-like modes),^{19,46} and they are dominantly coupled to HH exciton states in the QW. No higher-order modes of the slab waveguide are present for this structure in the frequency range of Fig. 2(b). The first five photonic bands are labelled with integer numbers. Mode 1 and part of mode 2 lie below the air light line and are therefore truly guided. In principle, such modes have infinite lifetime, and can leak radiation out of the slab plane only due to disorder in the photonic structure,^{57,58} which we neglect in the present paper. On the contrary, the modes are quasi-guided when their dispersion falls above the light line in the first BZ. These modes are coupled to

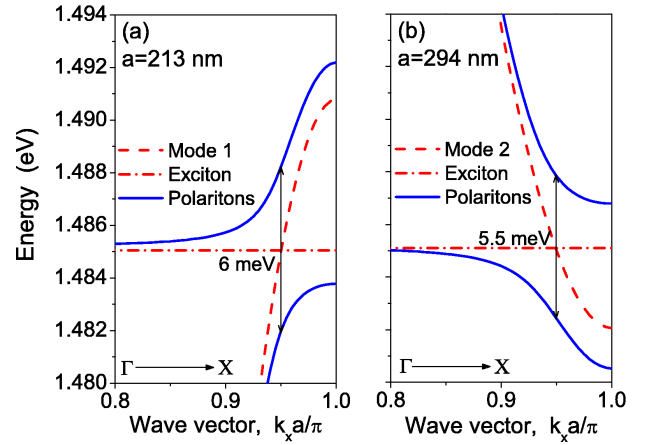


Figure 3: (color online) Guided polariton dispersion for a photonic mode interacting with a QW exciton at $E_{\text{ex}} = 1.485$ eV, close to the BZ edge (X -point); the uncoupled mode dispersions are shown with dashed and dot-dashed lines, respectively. Parameters of the photonic structure are: $r/a = 0.34$, $d/a = 0.3$. Panel (a): coupling to the first photonic mode, lattice constant $a = 213$ nm. Panel (b): coupling to the second mode, $a = 294$ nm.

the continuum of radiative PhC modes at the same energy. Physically, quasi-guided modes are lossy due to out-of-plane diffraction, thus acquiring a finite radiative linewidth $2\gamma_{kn}$ as discussed in Subsec. III A and calculated by the GME method.

We consider a single QW grown exactly in the middle of the GaAs layer, which maximizes coupling to the electric field for fundamental slab modes with even parity. The oscillator strength per unit area will be assumed to be $f/S = 4.2 \times 10^{12} \text{ cm}^{-2}$, typical of the HH exciton in an $\text{In}_x\text{Ga}_{1-x}\text{As}$ QW with thickness $L_{\text{QW}} = 8$ nm and low In content.^{3,4,59} The exciton energy is taken to be $E_{\text{ex}} = 1.485$ eV and the total exciton mass $M_{\text{ex}} = 0.18m_0$.⁴³ For the exciton linewidth we assume a value $2\gamma_{\text{ex}} = 1$ meV. Very high-quality QW structures can

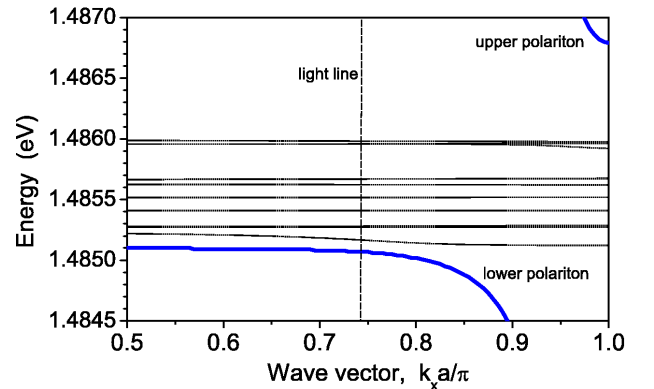


Figure 4: (color online) Close-up of Fig. 3(b) with exciton center-of-mass quantized levels explicitly shown.

be currently grown to achieve linewidths smaller than 0.5 meV. Here we stay on the conservative side, taking into account possible broadening induced by the presence of interface defects at the hole boundaries. These considerations are also supported by preliminary experimental data on square lattice PhC slabs with embedded QWs, which show no sizeable increase of the exciton linewidth as compared to an unpatterned area of the same sample (for an initial linewidth on the order of 2 meV).⁶⁰ With the parameters given here, the exciton-photon coupling matrix element calculated from Eq. (30) is on the order of a few meV, with slight variations depending on the photonic mode of interest, and the occurrence of strong or weak coupling for quasi-guided modes is governed by the photonic mode linewidth rather than by the exciton linewidth.⁶¹

A. Guided Polaritons

Due to the scalability of Maxwell equations, the PhC lattice can be engineered in order to have resonance between a given QW exciton energy and the desired photonic mode at any specific point in the BZ. When the exciton-photon resonance occurs below the light line (and the exciton linewidth is sufficiently small), the system is always in the strong coupling regime. The new quasi-particles that describe the eigenstates of the system are guided PhC polaritons, i.e., their photonic part is trapped within the high-index slab through total internal reflection.

In Fig. 3(a) and (b) we consider the interaction of a QW exciton with photonic modes 1 and 2 from the band dispersion shown in Fig. 2(b), respectively. The photonic lattice is engineered to have the resonance condition close to the BZ edge along the ΓX direction. In one case, the lattice constant is set to the value $a = 213$ nm, and in the other we assume $a = 294$ nm, so that the resonance at $E = 1.485$ eV is for $k_x \simeq 0.95\pi/a$ [see also arrows in Fig. 2(b)]. As it can be seen from Fig. 3, the dispersion of bare exciton and photon modes is strongly modified in both cases, giving rise to sizable anticrossings. It should be noted that in Fig. 3, as well as in the following figures of Secs. IV B and IV C, the uncoupled exciton center-of-mass levels are not explicitly shown. We rather prefer to show the bare exciton and photon dispersions as compared to the strongly coupled polaritonic dispersion. The calculated vacuum Rabi splitting is $\hbar\Omega_R = 6$ meV for the first mode and $\hbar\Omega_R = 5.5$ meV for the second one, respectively. The exciton-photon coupling is dependent on the specific band of interest, due to the different spatial profile of the corresponding electric field and thus to the modified overlap with the exciton center-of-mass wavefunctions. In any case, we point out that such values obtained with a *single* quantum well are comparable to those commonly achieved for MC polaritons with *six* QWs.⁴ The physical reason is the increased exciton-photon coupling of Eq. (30), due to better confinement

in the vertical direction of a high-index dielectric slab compared to a MC with low-index contrast distributed Bragg reflectors.

A close up of the dispersion diagram showing the center-of-mass quantized levels (with $M_{\max} = 10$) is given in Fig. 4, for parameters as in Fig. 3(b). It can be noticed that the quantization energy is $\lesssim 0.1$ meV in this specific case. These levels represent the effect of spatial dispersion, well known for bulk exciton-polaritons,⁴³ in the presence of center-of-mass quantization. Only the first few exciton levels are strongly interacting with the photonic mode of interest, due to symmetry of the corresponding envelope function and electric field. We point out that such effects cannot be captured by theoretical treatments based on a semiclassical solution of Maxwell's equations,^{23,24} in which the effect of spatial dispersion is neglected. Besides giving directly the dispersion of the mixed exciton-photon modes, the quantum theory developed here is also the starting point for studying polariton interactions and nonlinear processes, like in the case of bulk and microcavity systems.

B. Radiative Polaritons

When a QW exciton is resonant with a quasi-guided photonic mode, weak or strong coupling regimes may occur depending on the specific situation. We show in Fig. 5 the case of a PhC slab of lattice constant $a = 430$ nm, in which the exciton is resonant with different photonic modes within the first BZ [namely modes labelled with indices 4 and 5 in Fig. 2(b)]. In Fig. 5(a), the bare photonic mode dispersion around $E_{\text{ex}} = 1.485$ eV is shown. It is interesting to notice the existence of a photonic band minimum for mode 5 at the Γ point: such feature leads to a quasi-particle dispersion similar to MC polaritons, as it will be discussed. Actually, the resonance condition occurs simultaneously with different modes along ΓM and ΓX . In Fig. 5(b), the dispersion of the exciton-photon coupled modes is shown in a restricted energy range around the exciton resonance. Notice that there are five resonant points between QW excitons and PhC slab modes in the dispersion diagram, leading to a variety of situations for the coupled modes. Along ΓM , clear anticrossings can be seen with photonic modes 4 and 5, which are fingerprints of the strong coupling regime. In this case, the intrinsic radiative linewidth of bare photonic states is lower than the exciton-photon coupling energy. As the QW exciton is resonant with mode 4 for two different wave vectors along ΓM , we observe two anticrossings above the light line in the middle of the BZ. This peculiar effect is due to the light dispersion engineering allowed in PhC structures. Along ΓX , resonance with mode 5 gives strong coupling, while resonance with mode 4 at larger in-plane wave vector gives a crossing of the bare excitonic and photonic dispersions, meaning that the system is in weak coupling. We will analyze separately these distinct regimes in the following.

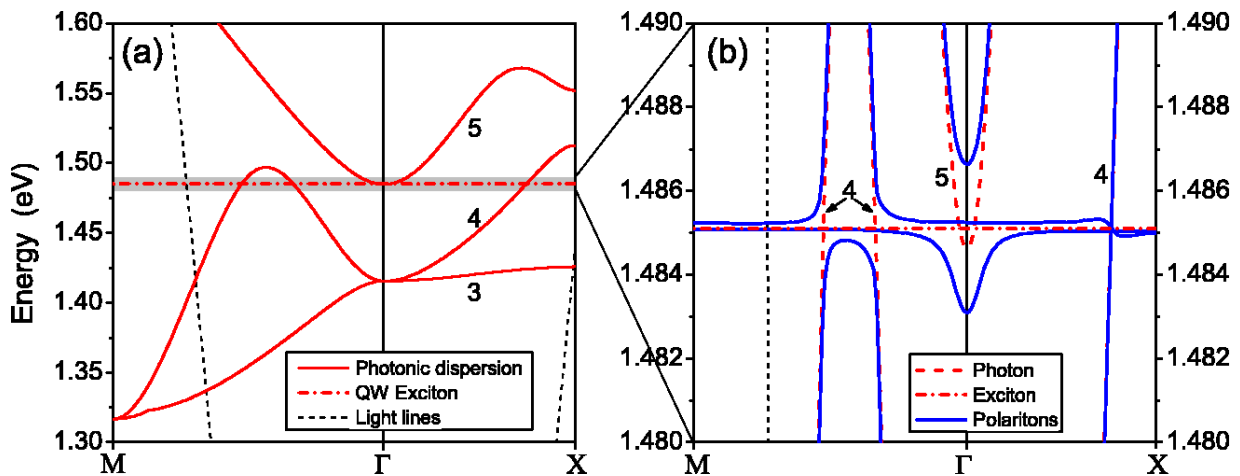


Figure 5: (color online) (a) Photonic mode dispersion around the QW exciton energy, $E_{\text{ex}} = 1.485$ eV, for structure parameters: $r/a = 0.34$, $d/a = 0.3$, $a = 430$ nm. (b) Close up for the 10 meV energy range of interest, showing the solution for the coupled exciton-photon system (full line) together with the bare exciton and photon dispersions (dashed).

We show in Fig. 6 the complex dispersion of the eigenmodes in the region of weak coupling, as compared to the bare QW exciton and photon energies. As seen in Fig. 6(a), photonic mode 4 is in weak coupling with all quantized exciton states (only one is shown here, for clarity) close to the X point. A slight modification of the exciton dispersion occurs close to resonance for the center-of-mass quantized mode having the same symmetry as the resonant photonic mode. The photonic mode dispersion is not perturbed at all by the presence of the QW. Remarkably, the plot of the intrinsic imaginary part calculated for the bare quasi-guided photonic mode in Fig. 6(b), evidences a linewidth close to $2\gamma_{\text{ph}} \sim 20$ meV, which explains the weak coupling regime for this particular case. Furthermore, the imaginary part of the photonic mode energy extracted from the solution of the Hopfield matrix shows no modification. On the contrary, and quite interestingly, the imaginary part of the QW exciton energy, initially set to $\gamma_{\text{ex}} = 0.5$ meV for the unperturbed state, is sensitively increased around the resonance. This indicates the occurrence of an enhancement of spontaneous emission rate or Purcell effect, which may be observed by time-resolved experiments.

In Fig. 7 we analyze the strong coupling regime above the light line, giving rise to radiative PhC polariton states. Mode 5 has a vanishing intrinsic linewidth at Γ [see imaginary part of the bare photonic mode in Fig. 7(b), dashed line], leading to a vacuum Rabi splitting. The real parts of the mode energies are shown around $\mathbf{k} = 0$ along the ΓM and ΓX symmetry directions. Looking at the bare QW exciton and mode 5 dispersions, we notice that the resonance condition is not exactly at Γ , but at small wave vectors ($|\mathbf{k}| \simeq 0.02\pi/a$). The exact resonant wave vector can be also inferred from Fig. 7(b), corresponding to the upper and lower polariton imaginary parts being coincident and equal to the average of bare exciton and photon values. As the bare

photonic linewidth goes to zero at Γ , the polariton imaginary part is about half of the bare QW exciton one at $\mathbf{k} = 0$. This *linewidth averaging* effect is well known for MC polaritons^{3,4} and is a fingerprint of the occurrence of a vacuum Rabi splitting.

C. Discussion and possible experimental verification

PhC slabs allow for a sensitive flexibility and tuning capability. In particular, a *lithographic tuning* (e.g., variation of the lattice constant or the air hole radius) on different devices patterned on the same chip is commonly used to ensure resonance of a desired mode with an active medium. Furthermore, techniques such as digital etching⁶² have been recently employed to achieve a fine tuning of photonic mode resonances. By using these post-processing techniques, it would be possible to tune the photonic mode of interest with respect to the QW exciton resonance. In Fig. 8 we show a simulation of such a procedure, in which the calculated detunings of the upper and lower polariton branches from the bare exciton resonance at $\mathbf{k} = 0$ are reported as a function of hole radius. The latter is slightly increased from $r/a = 0.336$ ($r \simeq 144.5$ nm) to $r/a = 0.344$ ($r \simeq 147.9$ nm). The typical anticrossing occurs exactly on resonance in the real part of energy, and the corresponding imaginary parts exchange each other from purely excitonic to purely photonic and viceversa. Concerning the significance of Fig. 8 with respect to state-of-the-art technological capabilities, wet chemical digital etching allows for deposition of a few monolayers of surface oxide that can be selectively removed, thus yielding a wavelength tuning of ~ 1 nm per etching cycle.⁶³ On the other hand, surface AFM oxidation of the PhC membrane can lead, in principle, to almost continuous tuning of the mode wavelength.⁶⁴

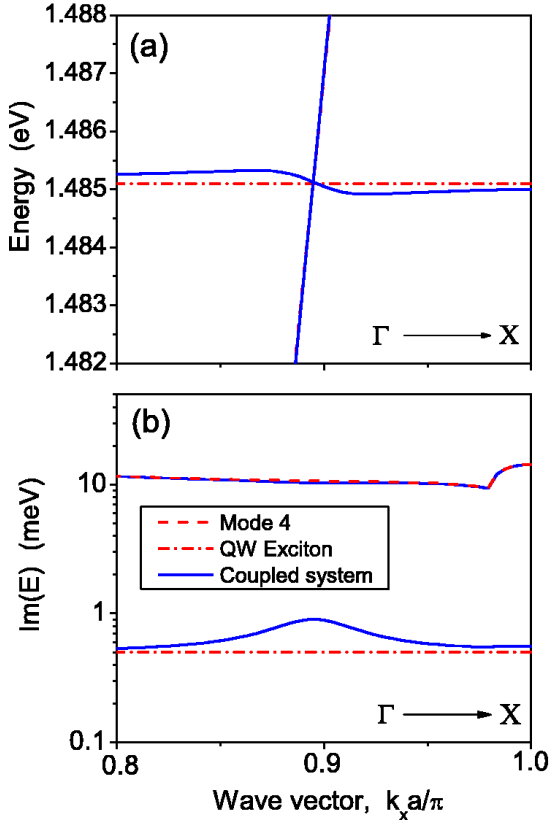


Figure 6: (color online) (a) Real and (b) imaginary parts of complex eigenenergies in the weak exciton-photon coupling regime close to the BZ edge along the ΓX direction. The bare exciton (dot-dashed) and photon (dashed) complex energies are also shown (the real part of photon dispersion nearly coincides with the coupled system solution). Structure parameters are as in Fig. 5.

Radiative PhC polaritons can be probed by angle-resolved reflectance from the sample surface, as first done on 1D PhCs filled with organic molecules.²² The same kind of experiment could be performed with semiconductor-based systems discussed in this work. Indeed, the present quantum-mechanical treatment of interacting photon and exciton states has been compared with semiclassical calculations of the surface reflectance, showing a very good agreement for the splitting in strong coupling regime.^{40,41,42} For guided polaritons, on the other hand, coupling to an external propagating beam is prohibited due to the evanescent character of the electromagnetic field in the claddings. In this case it would be possible to perform angle-resolved attenuated total reflectance by using a high-index prism. This technique was applied in Refs. 65,66 to probe the dispersion of pure photonic states in line-defect PhC waveguides.

We now focus on radiative properties close to $\mathbf{k} = 0$. As shown in Fig. 7, radiative polaritons can form with an energy minimum at the Γ point, due to the peculiar quasi-guided photonic mode dispersion in a square lat-

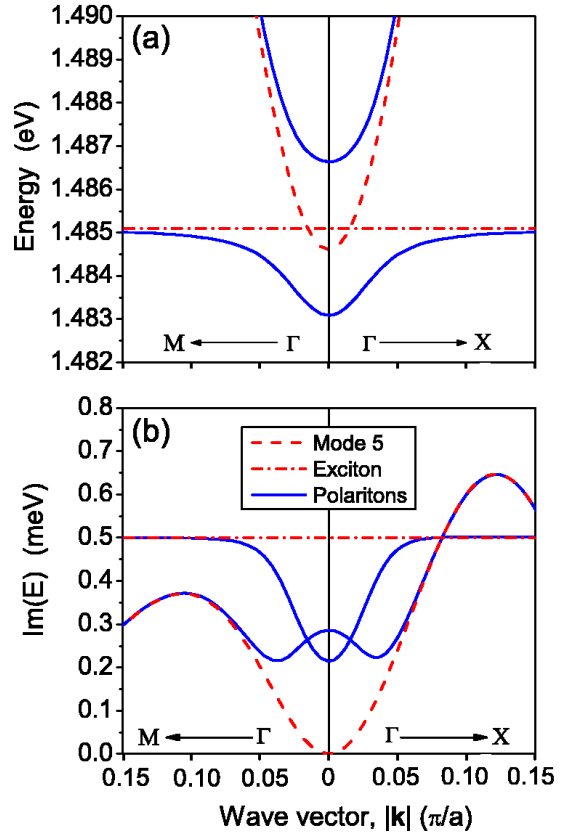


Figure 7: (color online) (a) Real and (b) imaginary parts of complex eigenenergies in the strong exciton-photon coupling regime close to normal incidence (Γ -point of the BZ) along the two main symmetry directions; the dispersion of uncoupled modes is also shown. Structure parameters are as in Fig. 5.

tice PhC membrane. The new eigenmodes of the system can be excited by coherent or incoherent pumping, and probed by emission or reflection at a fixed angle θ , which is defined in a vertical plane containing one of the high symmetry directions of the PhC lattice. A schematic picture of such an experimental configuration is shown in Fig. 9(a). The angle θ such that $k = (\omega/c) \sin \theta$, due to conservation of in-plane momentum. We consider here the angular dispersion along the ΓX direction for the case of zero-detuned (at normal incidence) bare exciton and photon modes. The calculated angular dispersion is shown in Fig. 9(b), in which we plot the energies of the upper and lower polariton branches detuned from the bare QW exciton energy (dot-dashed line). It is interesting to notice the similarities between the angular dispersion of Fig. 9(b) and the usual diagram used to illustrate the formation of a polariton trap in the energy minimum at $\mathbf{k} = 0$.⁵⁰ The peculiar properties of such an angular dispersion have been used in the last few years to achieve a number of outstanding results requiring non-linear parametric processes of MC polaritons.^{14,15,16} In particular, coherent population of the lowest energy polariton state at $\mathbf{k} = 0$ can be realized

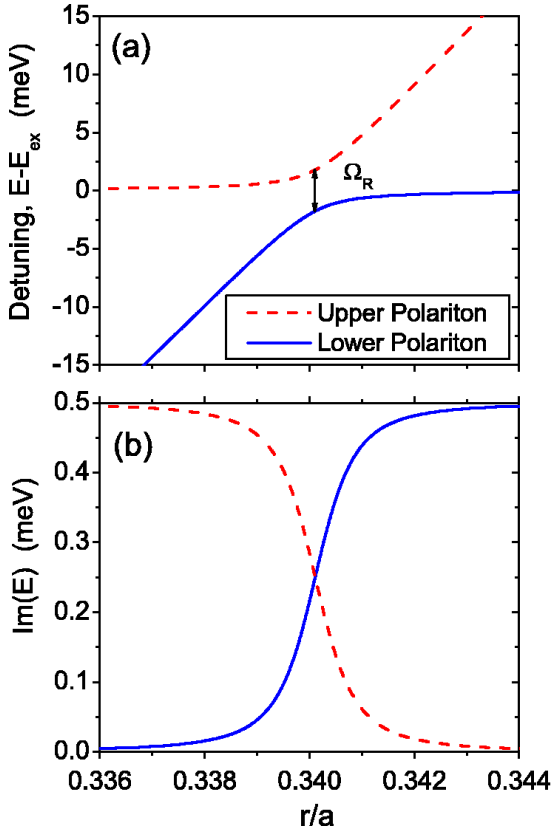


Figure 8: (color online) (a) Real and (b) imaginary parts of upper and lower polariton modes at $k = 0$ (Γ -point) as a function of hole radius. Structure parameters are as in Fig. 5.

by polariton-polariton scattering from a precise point in the dispersion, which allows for simultaneous energy and momentum conservation of the scattered quasi-particles. Similar experiments could be realized also with radiative PhC polaritons and a parametric process is schematically illustrated in the lower polariton branch of Fig. 9(b). An extension of the present theory to include nonlinear terms (such as exciton-exciton scattering)⁴⁹ in the hamiltonian represents a natural extension of this work. Moreover, the recent observation of the long-sought Bose-Einstein condensation of MC polaritons^{67,68} by use of II-VI materials¹⁶ has enhanced interest in low-dimensional polariton physics. The analogous effect in III-V materials, like InGaAs/GaAs, has not been observed at time of writing. A new route has been suggested to this end,⁶⁹ requiring efficient 0D confinement of MC polaritons through the confinement of their photonic part.⁷⁰ This is strong motivation for experimental as well as theoretical study of *PhC cavity polaritons*, in which ultra-high quality-factor and small mode volumes can be achieved and enhance the radiation-matter coupling in an unprecedented way.

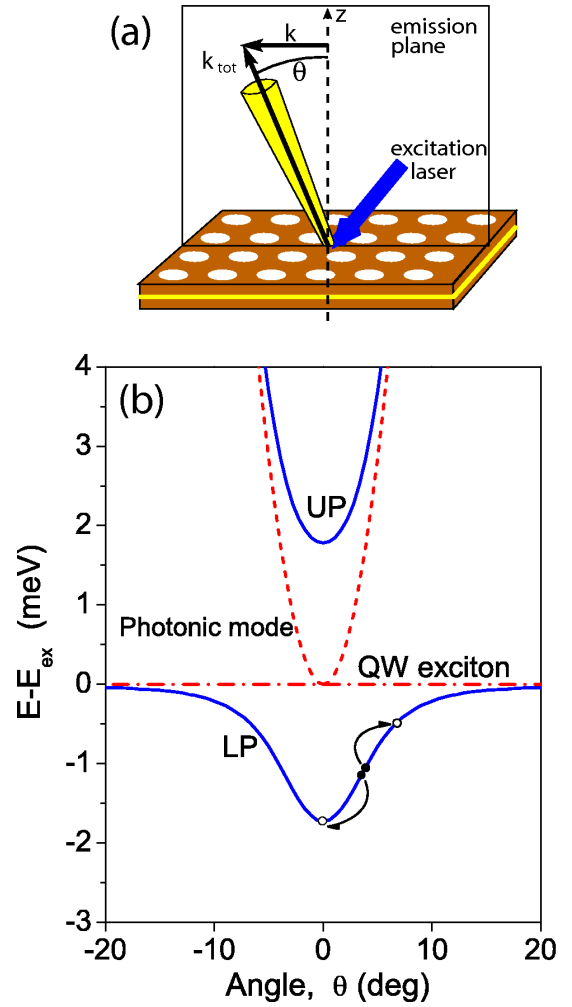


Figure 9: (color online) (a) Schematic view of angular emission from a PhC slab in a plane along a symmetry direction. The emission angle, $\theta = \arcsin(kc/\omega)$, is defined. (b) Calculated polariton angular dispersion in the ΓX direction, at zero bare exciton-photon detuning (see Fig. 8); a schematic polariton-polariton scattering process in the lower branch satisfying energy-momentum conservation is also shown.

V. CONCLUSIONS

In conclusion, we have presented a quantum theory to describe radiation-matter coupling for quantum wells embedded in a high-index photonic crystal slab with a generic pattern. The numerical solution of classical Maxwell equations, on which the present theory relies, has been previously reported within a guided-mode expansion approach⁴⁶ which yields not only the photonic mode energies but also the crucial photonic linewidth parameter. After obtaining the second-quantized total hamiltonian of the system in the linear regime of low excitation density, we have diagonalized it through a generalized Hopfield method. Thus, the complex eigenmodes of the exciton-photon coupled system have been

obtained. Both weak and strong coupling regimes are treated within the present theory, allowing for an efficient design of photonic lattices for specific purposes.

We have shown results on the square lattice PhC slab demonstrating the formation of guided and radiative photonic crystal polaritons. The latter are formed when the exciton-photon coupling exceeds the intrinsic photon linewidth. In strong coupling, the vacuum Rabi splitting at resonance is larger than for the corresponding microcavity polaritons, due to the increased field confinement and better overlap of exciton and photon wave fields in a PhC slab. As a consequence, a more robust polariton effect can be envisioned in such structures, which could be useful for nonlinear polariton applications. Related to the latter point, we reported on a specific lattice design for which the radiative polariton dispersion has a minimum around normal incidence. Such dispersion closely mimics the one obtained in usual microcavities, which acts as a polariton trap and is at the origin of current research on nonlinear parametric processes with exciton-polaritons. We believe that the present results will stimulate further research on non-linear polariton effects in semiconductor-based photonic crystals, which in turn could connect with polariton quantum optics^{71,72,73} as an emerging field of research.

Appendix A: GENERALIZED HOPFIELD METHOD

The Hopfield method to diagonalize the coupled exciton-photon hamiltonian is equivalent to performing

$$\begin{aligned}
\hbar\omega_n w_n + \sum_{n',\nu} 2D_{\nu nn'} w_{n'} - \sum_{n',\nu} 2D_{\nu nn'} y_{n'} - \sum_{\nu} iC_{n\nu} x_{\nu} - \sum_{\nu} iC_{n\nu} z_{\nu} &= \hbar\Omega w_n \\
&+ \sum_n iC_{n\nu} w_n - \sum_n iC_{n\nu} y_n + E_{\nu}^{(\text{ex})} x_{\nu} = \hbar\Omega x_n \\
\sum_{n',\nu} 2D_{\nu nn'} w_{n'} - \hbar\omega_n y_n - \sum_{n',\nu} 2D_{\nu nn'} y_{n'} - \sum_{\nu} iC_{n\nu} x_{\nu} - \sum_{\nu} iC_{n\nu} z_{\nu} &= \hbar\Omega y_n \\
- \sum_n iC_{n\nu} w_n + \sum_n iC_{n\nu} y_n - E_{\nu}^{(\text{ex})} z_{\nu} &= \hbar\Omega z_n.
\end{aligned} \tag{A2}$$

The sums in Eq. (A2) must be truncated in order to deal with finite matrices. If N_{max} photonic bands and M_{max} excitonic levels at fixed \mathbf{k} are retained in the expansion (33), the problem is reduced to an eigenvalue equation

$$\mathbb{M}\vec{\mathbf{v}} = \hbar\Omega\vec{\mathbf{v}}, \tag{A3}$$

where the matrix \mathbb{M} has dimension $2(N_{\text{max}} + M_{\text{max}}) \times 2(N_{\text{max}} + M_{\text{max}})$, and it is a generalization of the 4×4 matrix derived by Hopfield.¹⁰ The vector $\vec{\mathbf{v}}$ is simply

$$\vec{\mathbf{v}} = (w_n, x_{\nu}, y_n, z_{\nu})^{\text{T}}, \tag{A4}$$

a Bogoljubov transformation on bare exciton and photon operators. It was originally used by Hopfield for the case of bulk polaritons,¹⁰ and then generalized to polaritons in planar MCs^{30,34} and in micro-pillars.³⁵ Here we provide a detailed derivation of the generalized Hopfield matrix for the case of PhC slabs, which has to be diagonalized numerically. The second-quantized total hamiltonian, Eq. (32), and the polariton operator expansion, Eq. (33), are substituted in Eq. (35). The general commutation relations for bosonic operators

$$\begin{aligned}
[\hat{a}_{\mathbf{k}n}, \hat{a}_{\mathbf{k}'n'}^{\dagger} \hat{a}_{\mathbf{k}'n'}] &= \delta_{\mathbf{k},\mathbf{k}'} \delta_{n,n'} \hat{a}_{\mathbf{k}n} \\
[\hat{a}_{\mathbf{k}n}^{\dagger}, \hat{a}_{\mathbf{k}'n'}^{\dagger} \hat{a}_{\mathbf{k}'n'}] &= -\delta_{\mathbf{k},\mathbf{k}'} \delta_{n,n'} \hat{a}_{\mathbf{k}n}^{\dagger} \\
[\hat{a}_{\mathbf{k}n}, \hat{a}_{\mathbf{k}'n'} \hat{a}_{\mathbf{k}'n'}^{\dagger}] &= \delta_{\mathbf{k},\mathbf{k}'} \delta_{n,n'} \hat{a}_{\mathbf{k}n} \\
[\hat{a}_{\mathbf{k}n}^{\dagger}, \hat{a}_{\mathbf{k}'n'} \hat{a}_{\mathbf{k}'n'}^{\dagger}] &= -\delta_{\mathbf{k},\mathbf{k}'} \delta_{n,n'} \hat{a}_{\mathbf{k}n}^{\dagger}
\end{aligned} \tag{A1}$$

must be satisfied. Thus, after factorizing terms with common operators, the following system of linear equations in the variables w_n , y_n , x_{ν} , and z_{ν} can be derived (we drop the fixed subscript \mathbf{k} resp. $-\mathbf{k}$, for easier notation):

with $n = 1, \dots, N_{\text{max}}$, $\nu = 1, \dots, M_{\text{max}}$. The explicit form of the generalized Hopfield matrix is given by

$$\mathbb{M} = \begin{pmatrix} \omega + 2\mathbf{D} & -i\mathbf{C} & -2\mathbf{D} & -i\mathbf{C} \\ +i\mathbf{C} & \mathbf{E} & -i\mathbf{C} & \mathbf{0} \\ +2\mathbf{D} & -i\mathbf{C} & -\omega - 2\mathbf{D} & -i\mathbf{C} \\ -i\mathbf{C} & \mathbf{0} & +i\mathbf{C} & -\mathbf{E} \end{pmatrix}. \tag{A5}$$

The single blocks are respectively given by the $N_{\max} \times N_{\max}$ matrices

$$\boldsymbol{\omega} + 2\mathbf{D} = \llbracket \hbar\omega_n \delta_{n,n'} + \sum_{\nu} 2D_{\nu n n'} \rrbracket, \quad (\text{A6})$$

by the $M_{\max} \times M_{\max}$ diagonal matrices

$$\mathbf{E} = \llbracket E_{\nu}^{(\text{ex})} \delta_{\nu,\nu'} \rrbracket, \quad (\text{A7})$$

and by the $N_{\max} \times M_{\max}$ matrices

$$\mathbf{C} = \llbracket C_{n\nu} \rrbracket, \quad (\text{A8})$$

while $\mathbf{0}$ denotes the $M_{\max} \times M_{\max}$ matrix with zero entries. It should be noted that both positive- and negative-defined energy values are present in the Hopfield matrix. After the numerical diagonalization, yielding the eigenvalues $\hbar\Omega_p = E_p + i\gamma_p$, with $p = 1, 2, \dots, 2(N_{\max} + M_{\max})$, only those with positive real part are eventually retained.

ACKNOWLEDGMENTS

The authors are indebted with M. Agio for collaboration and for participating in the early comparisons between the present quantum formalism and calculations based on a semiclassical approach. They also acknowledge R. Ferrini and R. Houdré for useful discussions in the preliminary stages of the work concerning possible experimental realizations of the proposed structure. D. G. gratefully acknowledges C. Ciuti, H. Türeci, and A. Imamoğlu for insightful discussions, and A. Badolato, K. Hennessy, and M. Winger for preliminary experimental results.

* Present affiliation: Institute of Quantum Electronics, ETH Zurich. Email address: gerace@phys.ethz.ch.

¹ For a recent review: *Electron and Photon Confinement in Semiconductor Nanostructures*, edited by B. Deveaud, A. Quattropani, and P. Schwendimann (IOS Press, Amsterdam, 2003).

² G. Björk, S. Machida, Y. Yamamoto, and K. Igeta, *Phys. Rev. A* **44**, 669 (1991).

³ C. Weisbuch, M. Nishioka, A. Ishikawa, and Y. Arakawa, *Phys. Rev. Lett.* **69**, 3314 (1992).

⁴ R. Houdré, C. Weisbuch, R. P. Stanley, U. Oesterle, P. Pelandini, and M. Ilegems, *Phys. Rev. Lett.* **73**, 2043 (1994); R. Houdré, R. P. Stanley, U. Oesterle, M. Ilegems, and C. Weisbuch, *Phys. Rev. B* **49**, 16761 (1994).

⁵ M. S. Skolnick, T. A. Fisher, and D. M. Whittaker, *Semicond. Sci. Technol.* **13**, 645 (1998).

⁶ G. Khitrova, H. M. Gibbs, F. Jahnke, M. Kira, and S. W. Koch, *Rev. Mod. Phys.* **71**, 1591 (1999).

⁷ V. Savona, in *Confined Photon Systems - Fundamentals and Applications*, edited by H. Benisty, J.-M. Gérard, R. Houdré, J. Rarity, and C. Weisbuch (Springer, Berlin, 1999), p. 173.

⁸ A. Kavokin and G. Malpuech, *Cavity Polaritons* (Elsevier, Amsterdam, 2003).

⁹ L. C. Andreani, in *Electron and Photon Confinement in Semiconductor Nanostructures*, edited by B. Deveaud, A. Quattropani, and P. Schwendimann (IOS Press, Amsterdam, 2003), p. 105.

¹⁰ J. J. Hopfield, *Phys. Rev.* **112**, 1555 (1958).

¹¹ V. M. Agranovich, *J. Exp. Theor. Phys.* **37**, 430 (1959) [*Sov. Phys. JETP* **37**, 307 (1960)].

¹² C. F. Klingshirn, *Semiconductor Optics* (Springer, Berlin, 1995).

¹³ P. Yu and M. Cardona, *Fundamentals of Semiconductors* (Springer, Berlin, 1996).

¹⁴ P. G. Savvidis, J. J. Baumberg, R. M. Stevenson, M. S. Skolnick, D. M. Whittaker, and J. S. Roberts, *Phys. Rev. Lett.* **84**, 1547 (2000).

¹⁵ M. Saba, C. Ciuti, J. Bloch, V. Thierry-Mieg, R. André, Le Si Dang, S. Kundermann, A. Mura, G. Bongiovanni, J. L. Staehli, and B. Deveaud, *Nature (London)* **414**, 731 (2001).

¹⁶ J. Kasprzak, M. Richard, S. Kundermann, A. Baas, P. Jeambrun, J. M. J. Keeling, F. M. Marchetti, M. H. Szymańska, R. André, J. L. Staehli, V. Savona, P. B. Littlewood, B. Deveaud, and Le Si Dang, *Nature (London)* **443**, 409 (2006).

¹⁷ E. Yablonovitch, *Phys. Rev. Lett.* **58**, 2059 (1987).

¹⁸ K. Sakoda, *Optical Properties of Photonic Crystals* (Springer, Berlin, 2001).

¹⁹ S. G. Johnson and J. D. Joannopoulos, *Photonic Crystals: The Road from Theory to Practice* (Kluwer Academic Publishers, Boston, 2002).

²⁰ *Photonic Crystals: Advances in design, fabrication and characterization*, edited by K. Busch, S. Lölkes, R. B. Wehrspohn, and H. Föll (Wiley-VCH, Berlin, 2004).

²¹ For a recent review: *Photonic Crystals: Towards Nanoscale Photonic Devices*, edited by J.-M. Lourtioz, H. Benisty, V. Berger, J.-M. Gérard, D. Maystre, and A. Tchelnokov (Springer-Verlag, Berlin, 2005).

²² T. Fujita, Y. Sato, T. Kuitani, and T. Ishihara, *Phys. Rev. B* **57**, 12428 (1998).

²³ A. L. Yablonskii, E. A. Muljarov, N. A. Gippius, S. G. Tikhodeev, T. Fujita, and T. Ishihara, *J. Phys. Soc. Jpn.* **70**, 1137 (2001).

²⁴ R. Shimada, A. L. Yablonskii, S. G. Tikhodeev, and T. Ishihara, *IEEE J. Quantum Electron.* **38**, 872 (2002).

²⁵ S. Nojima, *Phys. Rev. B* **57**, R2057 (1998); *Phys. Rev. B* **59**, 5662 (1999).

²⁶ K. C. Huang, P. Bienstman, J. D. Joannopoulos, K. A. Nelson, and S. Fan, *Phys. Rev. Lett.* **90**, 196402 (2003); *Phys. Rev. B* **68**, 75209 (2003).

²⁷ E. L. Ivchenko, Y. Fu, and M. Willander, *Phys. Solid State* **42**, 1756 (2000).

²⁸ A. N. Poddubnyĭ, *Phys. Solid State* **49**, 360 (2007).

²⁹ R. Eichmann, B. Pasenow, T. Meier, T. Stroucken,

- P. Thomas, and S. W. Koch, Phys. Status Solidi B **238**, 439 (2003).
- ³⁰ V. Savona, Z. Hradil, A. Quattropani, and P. Schwendimann, Phys. Rev. B **49**, 8774 (1994).
- ³¹ S. Jorda, Phys. Rev. B **50**, 2283 (1994).
- ³² D. S. Citrin, IEEE J. Quantum Electron. **30**, 997 (1994).
- ³³ S. Pau, G. Björk, J. Jacobson, H. Cao, and Y. Yamamoto, Phys. Rev. B **51**, 14437 (1995).
- ³⁴ S. Savasta and R. Girlanda, Phys. Rev. A **53**, 2716 (1996).
- ³⁵ G. Panzarini and L. C. Andreani, Phys. Rev. B **60**, 16799 (1999).
- ³⁶ C. K. Carniglia and L. Mandel, Phys. Rev. D **3**, 280 (1971).
- ³⁷ R. J. Glauber and M. Lewenstein, Phys. Rev. A **43**, 467 (1991).
- ³⁸ S. T. Ho, L. Wang, and S. Park, in *Confined Photon Systems - Fundamentals and Applications*, edited by H. Benisty, J.-M. Gérard, R. Houdré, J. Rarity, and C. Weisbuch, (Springer, Berlin, 1999), p. 243.
- ³⁹ N. A. R. Bhat and J. E. Sipe, Phys. Rev. A **73**, 63808 (2006).
- ⁴⁰ D. Gerace, M. Agio, and L. C. Andreani, Phys. Status Solidi C **1**, 446 (2004).
- ⁴¹ L. C. Andreani, D. Gerace, and M. Agio, Photonics Nanostruct. Fundam. Appl. **2**, 103 (2004).
- ⁴² L. C. Andreani, D. Gerace, and M. Agio, Phys. Status Solidi B **242**, 2197 (2005).
- ⁴³ L. C. Andreani in: *Confined Electrons and Photons-New Physics and Devices*, edited by E. Burstein and C. Weisbuch (Plenum Press, New York, 1995), p. 57.
- ⁴⁴ A more general condition is that the photon dimensionality be lower than that of the exciton: see, e.g., the discussion in Ref. 9.
- ⁴⁵ C. Cohen-Tannoudji, J. Dupont-Roc, G. Grynberg, *Photons and Atoms, Introduction to Quantum Electrodynamics*, (Wiley, New York, 1997), p. 112.
- ⁴⁶ L. C. Andreani and D. Gerace, Phys. Rev. B **73**, 235114 (2006).
- ⁴⁷ F. Tassone and Y. Yamamoto, Phys. Rev. B **59**, 10830 (1999).
- ⁴⁸ G. Rochat, C. Ciuti, V. Savona, C. Piermarocchi, A. Quattropani, and P. Schwendimann, Phys. Rev. B **61**, 13856 (2000).
- ⁴⁹ C. Ciuti, P. Schwendimann, B. Deveaud, and A. Quattropani, Phys. Rev. B **62**, R4825 (2000).
- ⁵⁰ C. Ciuti, P. Schwendimann, and A. Quattropani, Semicond. Sci. Technol. **18**, S279 (2003).
- ⁵¹ We are assuming that the center-of-mass wavefunction can still be factorized when a photonic pattern is present. This is true provided the relative wavefunction is not modified when the exciton approaches the air holes, i.e., when dead-layer effects can be ignored. The assumption is reasonable as the exciton Bohr radius is much smaller than the typical scale of the photonic lattice.
- ⁵² R. Girlanda, A. Quattropani, and P. Schwendimann, Phys. Rev. B **24**, 2009 (1981).
- ⁵³ Notice that in the following we are assuming \mathbf{A} and \mathbf{p} to commute. Indeed, the additional terms arising from non-commutativity depend on the gradient $\nabla\epsilon(\mathbf{r})$ of the dielectric function, which vanishes inside the dielectric regions. The surface term at the hole sidewalls can also be dropped, because the exciton center-of-mass wavefunction vanishes at the hole boundaries in the limit $V_\infty \rightarrow \infty$.
- ⁵⁴ The phases of the fields have to be such that $C_{-\mathbf{k}\nu\nu} = C_{\mathbf{k}\nu\nu}^*$. This condition is fulfilled by the GME implementation used here.
- ⁵⁵ We notice that under this approximation the term proportional to \mathbf{A}^2 , which gives rise to the hamiltonian reported in Eq. 26, has negligible effect on the energy shift of mixed exciton-photon modes.³⁰ Such term is included here for completeness, as well as to highlight the similarities between the present formalism and the original one by Hopfield¹⁰ for bulk exciton-polaritons.
- ⁵⁶ In order to compare Eq. (31) with the exciton-photon coupling matrix element calculated, e.g., in Refs. 30,35, we notice that the expression for the overlap integral given here has dimensions $1/\sqrt{L}$, and it already contains the effects of vertical confinement on the electric field profile.
- ⁵⁷ D. Gerace and L. C. Andreani, Opt. Lett. **29**, 1897 (2004).
- ⁵⁸ D. Gerace and L. C. Andreani, Photonics Nanostruct. Fundam. Appl. **3**, 120 (2005).
- ⁵⁹ R. C. Iotti and L. C. Andreani, Phys. Rev. B **56**, 3922 (1997).
- ⁶⁰ A. Badolato, D. Gerace, K. Hennessy, M. Winger, and A. Imamoğlu (unpublished).
- ⁶¹ In the numerical calculations shown in the present work, convergence of photonic modes is achieved by using 101 plane waves and 2 guided modes in the basis set for GME. The number of exciton levels taken in the Hopfield matrix is typically $M_{\max} \leq 10$, which is largely sufficient to reach convergence for Rabi splitting with the photonic modes considered. A typical computation takes only a few minutes on a Personal Computer.
- ⁶² A. Badolato, K. Hennessy, M. Atatüre, J. Dreiser, E. Hu, P. M. Petroff, and A. Imamoğlu, Science **308**, 1158 (2005).
- ⁶³ K. Hennessy, A. Badolato, A. Tamboli, P. M. Petroff, E. Hu, M. Atatüre, J. Dreiser, and A. Imamoğlu, Appl. Phys. Lett. **87**, 21108 (2005).
- ⁶⁴ K. Hennessy, C. Högerle, E. Hu, A. Badolato, and A. Imamoğlu, Appl. Phys. Lett. **89**, 41118 (2006).
- ⁶⁵ M. Galli, M. Belotti, D. Bajoni, M. Patrini, G. Guizzetti, D. Gerace, M. Agio, L. C. Andreani, and Y. Chen, Phys. Rev. B **70**, 081307(R) (2004).
- ⁶⁶ M. Galli, D. Bajoni, M. Patrini, G. Guizzetti, D. Gerace, L. C. Andreani, M. Belotti, and Y. Chen, Phys. Rev. B **72**, 125322 (2005).
- ⁶⁷ A. Imamoğlu, R. J. Ram, S. Pau, and Y. Yamamoto, Phys. Rev. A **53**, 4250 (1996).
- ⁶⁸ D. Porras, C. Ciuti, J. J. Baumberg, and C. Tejedor, Phys. Rev. B **66**, 085304 (2002).
- ⁶⁹ V. Savona and D. Sarchi, Phys. Status Solidi B **242**, 2290 (2006).
- ⁷⁰ O. El Daïf, A. Baas, T. Guillet, J.-P. Brantut, R. Idrissi Kaitouni, J. L. Staehli, F. Morier-Genoud, and B. Deveaud, Appl. Phys. Lett. **88**, 61105 (2006).
- ⁷¹ C. Ciuti, Phys. Rev. B **69**, 245304 (2004).
- ⁷² K. Edamatsu, G. Oohata, R. Shimizu, and T. Itoh, Nature **431**, 167 (2004).
- ⁷³ S. Savasta, O. Di Stefano, V. Savona, and W. Langbein, Phys. Rev. Lett. **94**, 246401 (2005).